Research Article

Yanuar Rohmat Aji Pradana*, Aldi Ferara, Aminnudin Aminnudin, Wahono Wahono, and Jason Shian-Ching Jang

The Effect of Discharge Current and Pulse-On Time on Biocompatible Zr-based BMG Sinking-EDM

https://doi.org/10.1515/eng-2020-0049
Received Jan 06, 2020; accepted Mar 10, 2020

Abstract: The machinability information of Zr-based bulk metallic glasses (BMGs) are recently limited but essential to provide technological recommendation for the fabrication of the medical devices due to the material's metastable nature. This study aims to investigate the material removal rate (MRR) and surface roughness under different current and pulse-on time of newly developed Ni- and Cu-free Zr-based BMG using sinking-electrical discharge machining (EDM). By using weight loss calculation, surface roughness test and scanning electron microscopy (SEM) observation on the workpiece after machining, both MRR and surface roughness were obtained to be increased up to 0.594 mm^3/min and 5.50 μm, respectively, when the higher current was applied. On the other hand, the longer pulse-on time shifted the R_a into the higher value but lower the MRR value to only 0.183 mm^3/min at 150 μs. Contrary, the surface hardness value was enhanced by both higher current and pulse-on time applied during machining indicating different level of structural change after high-temperature spark exposure on the BMG surface. These phenomena are strongly related to the surface evaporation which characterize the formation of crater and recast layer in various thicknesses and morphologies as well as the crystallization under the different discharge energy and exposure time.

Keywords: Biocompatible Zr-based BMG, Sinking-EDM, Discharge current, Pulse-on time

***Corresponding Author: Yanuar Rohmat Aji Pradana:** Department of Mechanical Engineering, Universitas Negeri Malang, Malang City, 65145, Indonesia; Email: yanuar.rohmat.ft@um.ac.id
Aldi Ferara, Aminnudin Aminnudin, Wahono Wahono: Department of Mechanical Engineering, Universitas Negeri Malang, Malang City, 65145, Indonesia
Jason Shian-Ching Jang: Institute of Materials Science and Engineering, National Central University, Chungli, 320, Taiwan; Department of Mechanical Engineering, National Central University, Chungli, 320, Taiwan

1 Introduction

During the development, Zr-based bulk metallic glasses (BMGs) becomes most favourable alloy to be largely applied on several fields because of their excellences, such as high glass-forming ability (GFA), high fracture strength, low surface roughness (due to the absence of grain boundary), low Young's modulus, high recovery rate, good corrosion and wear resistance [1, 2]. By these unique properties, Zr-based BMG system is considered as potential material for biomedical application, even compared with Ti-based BMG. Although Ni and Be element, which are considered as harmful elements for human body, were successfully excluded in order to apply the alloy on medical application as reported by several researches, the other toxic element in the form of Cu was still involved into the alloy composition to sustain the GFA of BMG [3–5]. Moreover, the Cu ions released at the human body after implantation showed greater cytotoxicity potential than those of Be and Ni [6]. Because of this issue, the highly biocompatible Zr-based BMG with the alloy configuration of $Zr_{54}Al_{17}Co_{29}$ was designed and fabricated into 6 mm-diameter rod [7]. Although the alloy possessed lower GFA than toxic-containing Zr-based BMG, the mechanical and chemical characteristics were still superior, with the average hardness of 540 HV, fracture strength of 2220 MPa, plastic strain of 2 %, Young's modulus of 101 GPa, and better protective film-forming ability than SS 316L indicating this material can be formed into high-quality medical devices such as surgical blade and orthopedic drill bits previously fabricated by Jang Group [8, 9].

The problem for subsequent processing the advance materials with such high mechanical properties is that the material becomes difficult to be machined. Several studies implied the limitation to cut BMG using conventional machining at dry condition, namely high cutting forces, high cutting temperature, and excessive tool wear [10, 11]. The high cutting forces and temperature can induce crystallization on amorphous body occurred on both machined surface and chip, subsequently deteriorate the amorphous nature of materials and lower its application [12, 13]. De-

spite the fact that the problem can be minimized by applying lower cutting speed and cutting fluid during machining, but for processing $Zr_{54}Al_{17}Co_{29}$ BMG having low GFA (compared with BMG used on the preceding studies), the crystallization tends to occur easily through conventional machining.

Electrical-based nonconventional machining such as electrical discharge machining (EDM) is possibly applied to cut BMG by substituting shearing material removal mechanism on conventional machining because BMG performed better electrical conductivity compared with that on oxide glass material. Different from laser- [14] and plasma-based [15] processing having no cooling system, dielectric fluid applied on EDM acts not only as insulator from high density of spark exposure at nearest gap between tool and workpiece during material removal mechanism but also as cooling system of the tool and machined surface; therefore, it increases the possibility of cutting heat localization and thus limit the crystallization of the BMG at the lower level than those on conventional machining [16]. As reported before, spark occurred during machining characterized the discharge energy transmitted on the workpiece surface and became the dominant driving parameter for material removal mechanism on EDM cutting, beside of the dielectric flushing system [17]. Nowadays, micro-EDM was preferable to be applied in order for avoiding crystallization of BMG cutting because of its low discharge energy, based on several reports [18, 19]; however, the method is considered inappropriate for cutting macro-dimensional shape on medical devices; therefore another technique is needed to cut BMG at a larger scale.

Among the other determining factors on EDM (dielectric and tool), machining parameters become a most flexible factor in modifying the EDM performance on BMG cutting, where polarity, current, and pulse-on time in the sequence were reported to be top-three of the most influential factors on material removal as described by Mathumaringam [16]. Although considered as the dominant factor, polarity adjustment is not applicable to be adjusted on all EDM machine types due to limited feature on these machines. However, in this case, these parameters need to be selected and combined properly by also considering the crystallization occurred on BMG workpiece due to high discharge energy, besides the material removal rate (MRR) and surface quality to maintain the material unique properties which rarely done on biocompatible BMG material by other researchers. In this study, the role of EDM process parameters, in the form of discharge current and pulse-on time, on the MRR, surface roughness and hardness evolution of biocompatible $Zr_{54}Al_{17}Co_{29}$ BMG sinking-EDM were investigated using weight loss calculation, surface roughness test, and microvickers hardness test. To confirm the surface morphology after machining, the microstructural observation was conducted by scanning electron microscopy (SEM) at various magnifications. The experimental results were then analyzed and discussed to provide the technological recommendation for further application.

2 Materials and Methods

In this study the BMG sample was provided by High-Performance Alloy Laboratory, NCU, Taiwan with the alloy configuration of $Zr_{54}Al_{17}Co_{29}$ (in at.%) owing the density of 6.52×10^{-3} g/mm^3 in the form of a rod having diameter and length of 4 and 80 mm, respectively. A 100 mm-long cylindrical CuCr rod having a diameter of 10 mm was used as tool material. Both the BMG rod and tool cross-sectional surfaces were then flattened and polished to ensure the parallel gap between their interface using a centrifugal sandpaper machine. Before machining, the CuCr tool and BMG workpiece were also polished using similar grit of sandpaper to ensure the similar surface roughness level on the both workpiece and tool cross section for each experiment stage. The machining was conducted using C-TEK ZNC 320 EDM Machine by varying the discharge current and pulse-on time. Due to the larger area of the tool compared with the workpiece, the machining was subjected completely on all area of BMG top surface. The machining condition was completely listed in Table 1. During the process, the BMG - tool gap was insulated and cooled by oil-based dielectric fluid (Chevron HONILO 409) applying jet flushing mode. Digital scale (OPTIMA OPD-E204) was used to measure the weight difference between BMG workpiece before and after machining for material removal rate calculation.

The surface roughness of BMG workpiece formed after machining was evaluated using surface roughness tester (MITUTOYO Surface SJ 301 Series) and the test was taken on 3 different locations of each workpiece to make sure the result validity. To investigate the structural change on the newly developed layer of BMG workpiece machined surface, the microvickers hardness (ESEWAY) test was conducted using the indentation load and period of 500 g and 10 s, respectively. The indentation was also subjected to 3 different locations on the sample surface. The scanning electron microscopy (SEM) observation (PHENOM G2 Pro) was also conducted to evidence the morphological condition and thickness of the recast layer developed on the BMG surface after machining using different machining

parameter combination. The SEM image was taken at the magnification of 200, 500, and 1000 times.

Table 1: Experimental conditions for biocompatible Zr-based BMG machining by EDM

Parameter	Value
Workpiece	
Material	$Zr_{54}Al_{17}Co_{29}$ BMG rod
Diameter (mm)	4
Density (g/mm^3)	6.52×10^{-3}
Tool	
Material	CuCr
Diameter (mm)	10
Machining parameter	
Polarity	Electrode (+)
Depth of cut (mm)	0.2
Retract distance (mm)	8
Gap voltage (V)	40
Tool-workpiece gap (mm)	0.1
Pulse-off time (μs)	4
Discharge current (A)	4, 8, 12
Pulse-on time(μs)	50, 100, 150
Dielectric	
Oil	Chevron HONILO 409
Flash point (°C)	116
Viscosity (CST)	5.7
Flushing mechanism	Jet flushing

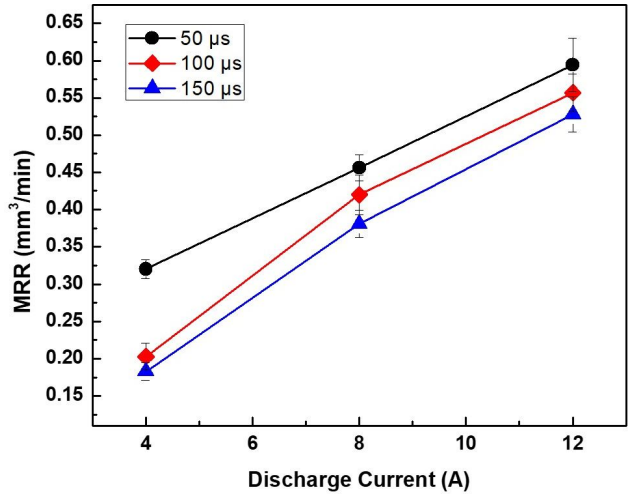

(a)

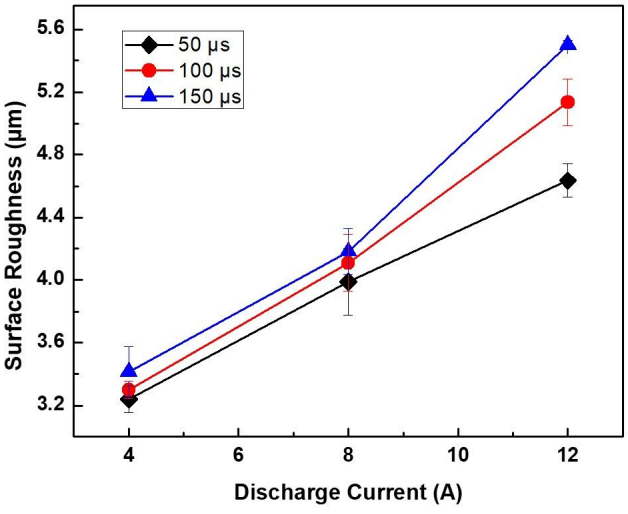

(b)

Figure 1: (a) MRR curves of BMG machined surface varied by discharge current and pulse-on time and (b) surface roughness curves of BMG machined surface varied by discharge current and pulse-on time of BMG sinking EDM

3 Results and Discussions

3.1 Material Removal Rate

The MRR was defined as the material loss in the unit of volume for certain machining time on BMG sample using selected discharge current and pulse-on time combination. The equation is described as follow (1).

$$MRR = \frac{W_{BW} - W_{AW}}{t \times \rho_w} \quad (1)$$

Where w_{BW} is workpiece weight before machining (g), w_{AW} is workpiece weight after machining (g), t is machining time (min), and ρ_w is workpiece density (g/mm^3)

Figure 1(a) shows the relation between discharge current and MRR using various pulse-on time values, where the MRR is observed to be higher, reaching the maximum value of 0.594 mm^3/min, when the larger discharge current was applied. The results indicate that the high current is more productive for BMG machining using EDM. The current represents discharge energy determining heat generation during spark material removal mechanism, where the melting and evaporation on the workpiece surface occurred at higher level induced by high discharge temperature. This phenomenon was also reported by previous studies [18, 19]. Additionally, by increasing discharge energy, the debris deposited in the tool-workpiece gap was also increased. The debris contains the dielectric decomposition product and eroded conductive BMG particles. As machining proceeds, the amount of particle increased rapidly at the gap. The particles can exert significant influence on the characteristics of dielectric breakdown and

influence the material removal mechanism [20]. Moreover, the short pulse-on time can induce the more opportunity for debris in the machining gap to be flushed away from the machining region by dielectric fluid during a similar period of pulse-off time thus resulting in higher MRR. This MRR is significantly higher compared with micro-EDM process subjected to machine micro-scale shape, as revealed by other researchers [16, 17].

On the other hand, from the figure, it can also be observed that the pulse-on time brings an inverse effect on MRR, where the higher MRR curve is achieved by shorter pulse-on time. For example, at the current of 4 mm, the MRR are 0.320; 0.203; and 0.183 mm^3/min at 50, 100, and 150 µs, respectively. This parameter showed the different effect compared with discharge current on the removal mechanism. The results are similar to the study reported by Mohan et al. [20]. Contrary, Wang and Yan found the different fact that MRR was increased along with the increase pulse-on time at lower range [21]. However, it turns to be decreased at a longer pulse-on time application. It indicates that the inverse effect of pulse-on time towards MRR can be achieved beyond their optimum condition. The short pulse-on time might induce low vaporization on the BMG workpiece surface, while the excessive pulse duration may cause an expansion of the plasma channel, thereby decreasing the energy density transmitted the machining process.

3.2 Surface Roughness

In this study, the BMG surface quality was strongly characterized by both discharge current and pulse-on time applied during machining. Figure 1(b) shows the surface roughness as a representative of surface quality is increased significantly at the highest value of 5.50 µm, if the higher current was applied, irrespective to the other parameter, indicating the deterioration on surface quality occurred when using high discharge energy during machining. This phenomenon is similar with those occured on previous studies where the increased discharge energy, which is proportional with the current, inducing the higher machining efficiency and the development of the larger size of the crater on the machined surface [18–20]. This larger crater size, correspond to the high amount of material melting during discharge mechanism (pulse-on time). When the crater size is similar, the randomly overlapped crater distribution can be the determining factor to characterize the surface roughness [23].

The different trend compared with MRR curve was obtained on surface roughness analysis varied by pulse-on

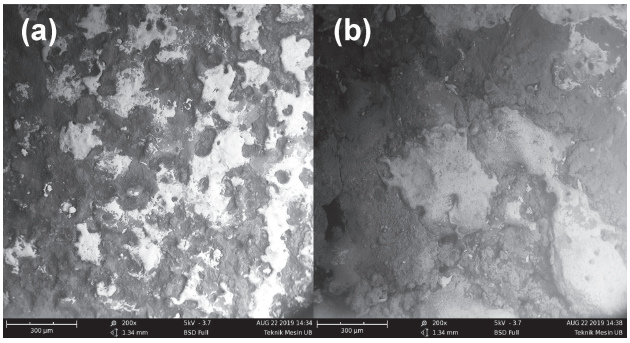

Figure 2: SEM images of BMG machined surface at (a) 4 A, 50 µs combination and (a) 12 A, 150 µs combination using 200 times magnification

time. According to Figure 1(b), it can be noticed that the higher surface roughness level is obtained by longer pulse-on time, where lowest surface roughness is obtained at the current of 4 A and pulse-on time of 50 µs with 3.24 µm, indicating the short pulse-on time was favourable for resulting high surface quality. In BMG EDM, the short pulse-on time might induce low vaporization on the BMG workpiece surface, due to its unique amorphous thermal behaviour. Eventually, the short pulse-on time produces a shallow crater on the surface of the workpiece resulting in better surface quality. This phenomenon was significantly different compared with the machining of crystalline metal such as SiC and Al alloy which showed an inverse relation between pulse-on time and surface roughness [20, 21]. During the pulse-on time, sparks arise at the gap between the tool and BMG workpiece, causing local heating, melting, and vaporization on both the BMG workpiece and tool. At the short pulse-on time, unlike the phenomenon occurred on the highly-conductive CuCr tool, these thermal cycle was occurred on BMG only at a low level, thus resulting in the small crater size.

In order to further analyze the surface roughness of BMG machined surface, the SEM observation was conducted on the workpiece having lowest (4 A, 50 µs) and highest (12 A, 150 µs) roughness of 3.24 and 5.5 µm, respectively, using the magnification of 200 and 500 times. Figure 3 indicates that the carbonaceous layer, produced from the breakdown of dielectric fluid [23, 24], was deposited on the machined surface. It is also clear that by using low on both current and pulse-on time, the crater size is clearly smaller (Figure 2(a)) than those on highest respective parameters ((Figure 2(b)) indicating the low current had a positive impact on reducing the surface roughness. Based on Figure 3, The average crater diameter on the lowest and highest surface roughness of BMG machined surface is measured at 165 and 400.9 µm, respectively. On

the other hand, the micro-porous was also found on the machined surface using 12 A and 150 µs, as shown in Figure 3 (b). The micro-porous was possibly formed by irregular overlapping craters distribution induced by excessive melting due to high discharge energy, as also stated by several other studies [18, 19, 23]. These crater size and micro-porous appearance were responsible on the increased surface roughness on machined BMG; therefore, when the surface quality becomes the essential criteria, such as a finishing step, the discharge energy should be maintained as low as possible.

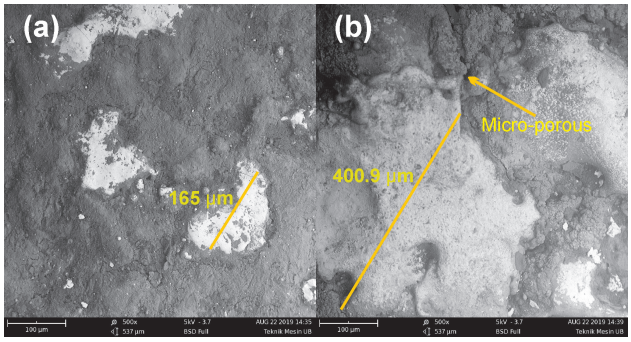

Figure 3: SEM images of BMG machined surface at (a) 4 A, 50 µs combination and (a) 12 A, 150 µs combination using 500 times magnification

3.3 Surface Hardness

Due to the difficulties to reveal the structural change by performing the XRD analysis on relatively rough $Zr_{54}Al_{17}Co_{29}$ BMG machined surface covered with a carbonaceous layer, the hardness test was conducted on the sample surface after machining to reveal the change of BMG surface mechanical properties. This effort was performed considering the importance of these structural issues on biocompatibility and chemical properties of BMG before application. Figure 4 describes the surface hardness curves varied by both current and pulse-on time where the increase of discharge current conducts a higher level of surface hardness. The hardness value ranges from 247.6 to 418.5 HV, and these values are significantly lower than the hardness of the as-cast amorphous sample of 541 HV. It indicates that the transformation of initial glassy structure in the form of crystallization may occurred at higher increment of high spark temperature resulted by high discharge energy. This issue was referred on our previous work conducted at BMG composition, where the crystallinity was increased by longer annealing time resulting in high hardness level on $Zr_{54}Al_{17}Co_{29}$ BMG due to the presence of hard intermetallic compounds [25]. The crystallization was also possibly contributed by a good chemical affinity of Zr and possibly appeared C atoms [19]. However, the crystallization phenomenon on annealing is different with the melting and re-solidifiction occurred on the BMG surface during discharge process, where at the annealing, the nanocrystals is formed and acted as strengthening phase to enhance the BMG mechanical properties, including the hardness. In this study, the crystallization is occured at higher level, or possibly fully-crystallization, at the BMG surface; therefore, it shows different effect on the hardness change as lower mechanical properties of crystalline alloy than its BMG counterpart. As comparison, for Be-, Ni-, and Cu-containing Zr-based BMGs in the form of $Zr_{41.2}Ti_{13.8}Cu_{12.5}Ni_{10}Be_{22.5}$ [19, 23] and $Zr_{55}Al_{10}Ni_5Cu_{30}$ [26], where these toxic elements act as GFA stabilizer, the crystallization is still occurred on the sample surface although the BMG samples are only cut by micro-EDM using low discharge energy. By considering this fact, the crystallization in this study should be occurred at higher level due to the lower GFA of $Zr_{54}Al_{17}Co_{29}$ (because of the absence of Be, Ni, and Cu elements) which is more sensitive and having lower ability to maintain the amorphous characteristics under the high discharge energy exposure exerted by conventional EDM process.

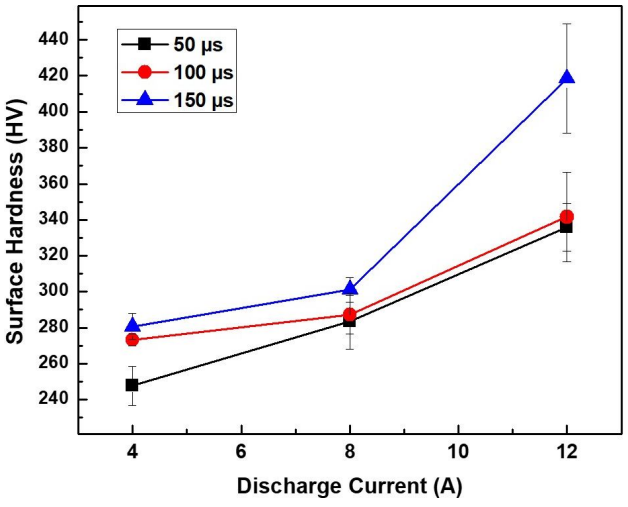

Figure 4: The relationship between discharge current and surface hardness of BMG machined surface under different pulse-on time condition

On the other hand, pulse-on time also played an important role to characterize the hardness where the longer pulse-on time is observed to enhance the surface hardness of the machined surface, as depicted in Figure 4.

This phenomenon is correlative with those obtained on the surface roughness analysis, where the change of pulse-of time related to the behaviour of developed recast layer after machining. The long pulse-on time induced high-temperature spark occurring at the tool-workpiece gap during the discharging process, causing local heating, melting, and vaporization at a high level resulting in higher crystallization on BMG machined surface. The thermal-induced-structural change is more susceptible to be appeared on BMG, in comparison with metallic material due to the low thermal stability (metastable nature) and more stages of phase transformation of glassy alloys [27].

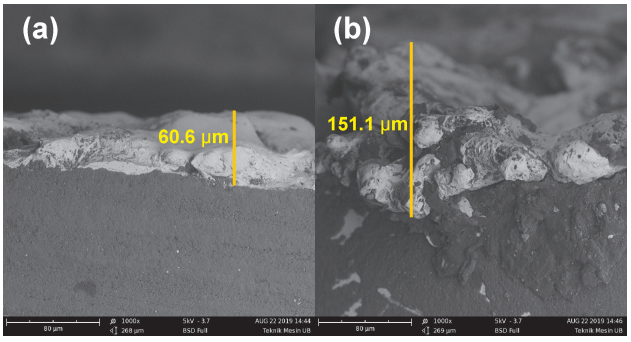

Figure 5: SEM images of side view on BMG machined surface at (a) 4 A, 50 µs combination and (a) 12 A, 150 µs combination using 1000 times magnification performing recast layer

Figure 5 shows the side view of the machined surface, demonstrating the thickness of formed recast layer on the top BMG surface. From Figure 5(a) it indicates that the thin recast layer of 60.6 µm was generated at low discharge energy, while the layer was increased significantly up to 151,1 µm using the highest discharge energy as depicted on Figure 5(b). Recast layer was formed from partially molten metal which was not involved in the evaporation process due to the cooling done by the dielectric. When the discharge energy is higher, the larger workpiece region is melted and evaporated, thus resulting in thicker recast layer. In the case of BMG sinking EDM, the thickness of recast layer formed becomes the indicator of the crystallization occurred on the amorphous body; therefore it can reduce the unique properties of BMG and thus considered as a limitation of BMG machining. The condition was then worsened by applying long pulse-on time because it does not only generate high discharge temperature, but also induces insufficient ejection force causing the part of ejection BMG to remain as a recast layer, and the process becomes evidence at stationary tool [20]; therefore, low discharge energy is needed to be selected to reduce the crystallization. However, the recast layer can be removed by a subsequent polishing process to maintain the glassy surface, as proposed by Huang [19].

4 Conclusion

Based on the experimental investigation, the important informations were obtained on the machinability of newly-deveoped biocompatible $Zr_{54}Al_{17}Co_{29}$ BMG, which is hard-to-cut and susceptible to crystallization, using the most determining process parameters of sinking-EDM and those are summarized as follows. The MRR reached a higher increment at higher discharge current and lower pulse-on time. The pulse-on time, showed the correlative relation with the surface roughness instead of inverse relation as largely found on the metallic material machining due to the metastable nature of common BMG. The surface roughness was characterized by the crater size and the presence of micro-porous, as confirmed by SEM. The different degree of hardness were found on the BMG machined surface, indicating the crystallization. The recast layer is considered as crystallization site of the glassy alloy. These results can be a technological recommendation for further EDM application on the metastable BMG materials for bio-implant and medical devices. The structural and corrosion analyses on the biocompatible Zr-based BMG machined surface need to be conducted for advanced study.

Acknowledgement: The authors express the gratitude to Universitas Negeri Malang for the financial support under the Research Funding of PNBP Academic Year 2019 (Contract No. 20.3.265/UN32.14.1/LT/2019). The authors are also thankful to High-Performance Alloy Laboratory, National Central University, Taiwan for preparing Biocompatible Zr-based BMG sample. Imam Sudjono and Agus Suyetno from Manufacturing Laboratory of Universitas Negeri Malang are also acknowledged for EDM technical supports.

References

[1] Inoue A, Zhang T. Fabrication of Bulk Glassy $Zr_{55}Al_{10}Ni_5Cu_{30}$ Alloy of 30 mm in Diameter by a Suction Casting Method. Mater Transitions 1996;37:185–7.

[2] Yang Y, Hua N, Li R, Pang S, Zhang T. High-zirconium bulk metallic glasses with high strength and large ductility. Sci China Physics, Mech Astron 2013;56:540–4. https://doi.org/10.1007/s11433-013-5015-7.

[3] Sun Y, Huang Y, Fan H, Liu F, Shen J, Sun J, et al. Comparison of mechanical behaviors of several bulk metallic glasses for biomedical application. J Non Cryst Solids 2014;406:144–50.

https://doi.org/10.1016/j.jnoncrysol.2014.09.021.
[4] Hua N, Huang L, Chen W, He W, Zhang T. Biocompatible Ni-free Zr-based bulk metallic glasses with high-Zr-content: Compositional optimization for potential biomedical applications. Mater Sci Eng C 2014;44:400–10. https://doi.org/10.1016/j.msec.2014.08.049.
[5] Espallargas N, Aune RE, Torres C, Papageorgiou N, Muñoz AI. Bulk metallic glasses (BMG) for biomedical applications—A tribocorrosion investigation of $Zr_{55}Cu_{30}Ni_5Al_{10}$ in simulated body fluid. Wear 2013;301:271–9. https://doi.org/10.1016/j.wear.2012.12.053.
[6] Elshahawy WM, Watanabe I, Kramer P. In vitro cytotoxicity evaluation of elemental ions released from different prosthodontic materials. Dent Mater 2009;25:1551–5. https://doi.org/10.1016/j.dental.2009.07.008.
[7] Li TH, Liao YC, Song SM, Jiang YL, Tsai PH, Jang JSC, et al. Significantly enhanced mechanical properties of ZrAlCo bulk amorphous alloy by microalloying with Ta. Intermetallics 2018;93:162–8. https://doi.org/10.1016/j.intermet.2017.12.008.
[8] Tsai PH, Lin YZ, Li JB, Jian SR, Jang JSC, Li C, et al. Sharpness improvement of surgical blade by means of ZrCuAlAgSi metallic glass and metallic glass thin film coating. Intermetallics 2012;31:127–31. https://doi.org/10.1016/j.intermet.2012.06.014.
[9] Li TH, Tsai PH, Hsu KT, Liu YC, Jang JSC, Huang JC. Significantly enhanced drilling ability of the orthopedic drill made of Zr-based bulk metallic glass composite. Intermetallics 2016;78:18–21. https://doi.org/10.1016/j.intermet.2016.08.001.
[10] Maroju NK, Yan DP, Xie B, Jin X. Investigations on surface microstructure in high-speed milling of Zr-based bulk metallic glass. J Manuf Process 2018;35:40–50. https://doi.org/10.1016/j.jmapro.2018.07.020.
[11] Chen X, Xiao J, Zhu Y, Tian R, Shu X, Xu J. Micro-machinability of bulk metallic glass in ultra-precision cutting. Mater Des 2017;136:1–12. https://doi.org/10.1016/j.matdes.2017.09.049.
[12] Bakkal M. Electron microscopy of bulk metallic glass machining chips. J Non Cryst Solids 2009;355:2220–3. https://doi.org/10.1016/j.jnoncrysol.2009.07.018.
[13] Ding F, Wang C, Zhang T, Zheng L, Zhu X. High performance cutting of Zr-based bulk metallic glass: a review of chip formation. Procedia CIRP 2018;77:421–4. https://doi.org/10.1016/j.procir.2018.08.294.
[14] Williams E, Lavery N. Laser processing of bulk metallic glass: A review. J Mater Process Technol 2017;247:73–91. https://doi.org/10.1016/j.jmatprotec.2017.03.034.
[15] Elaragi GM. Design and Operation of First Egyptian IEC Fusion Plasma Device. Emerg Sci J 2019;3:241–8. https://doi.org/10.28991/esj-2019-01186.
[16] Patel JD, Maniya KD. A Review on : Wire cut electrical discharge machining process for metal matrix composite. Procedia Manuf 2018;20:253–8.
[17] Muthuramalingam T, Mohan B. A review on influence of electrical process parameters in EDM process. Arch Civ Mech Eng 2015;15:87–94. https://doi.org/10.1016/j.acme.2014.02.009.
[18] Liu C, Duong N, Jahan MP, Ma J, Kirwin R. Experimental investigation and numerical simulation of micro-EDM of bulk metallic glass with focus on crater sizes. Procedia Manuf 2019;34:275–86. https://doi.org/10.1016/j.promfg.2019.06.151.
[19] Huang H, Yan J. Microstructural changes of Zr-based metallic glass during micro-electrical discharge machining and grinding by a sintered diamond tool. J Alloys Compd 2016;688:14–21. https://doi.org/10.1016/j.jallcom.2016.07.181.
[20] Mohan B, Rajadurai A, Satyanarayana KG. Effect of SiC and rotation of electrode on electric discharge machining of Al–SiC composite. J Mater Process Technol 2002;124:297–304. https://doi.org/10.1016/S0924-0136(02)00202-9.
[21] Wang CC, Yan BH. Blind-hole drilling of Al_2O_3/6061Al composite using rotary electro-discharge machining. J Mater Process Technol 2000;102:90–102. https://doi.org/10.1016/S0924-0136(99)00423-9.
[22] Taylor P, Muthuramalingam T, Mohan B. Influence of Discharge Current Pulse on Machinability in Electrical Discharge Machining. Mater and Manuf Process 2013:37–41. https://doi.org/10.1080/10426914.2012.746700.
[23] Huang H, Yan J. On the surface characteristics of a Zr-based bulk metallic glass processed by microelectrical discharge machining. Appl Surf Sci 2015;355:1306–15. https://doi.org/10.1016/j.apsusc.2015.08.239.
[24] Maradia U, Boccadoro M, Stirnimann J, Kuster F, Wegener K. Electrode wear protection mechanism in meso–micro-EDM. J Mater Process Technol 2015;223:22–33. https://doi.org/10.1016/j.jmatprotec.2015.03.039.
[25] Pradana YRA, Jang JS, Setyabudi SA. Mechanical properties transformation on $Zr_{54}Al_{17}Co_{29}$ bulk metallic glass by partial crystallization. J Rekayasa Mesin 2017;8:23–8.
[26] Zuo L, Pang S, Zou S, Li H, Zhang T. Surface vitrification of alloys by pulsed electrical discharge treatment. J Alloys Compd 2017;707:148–54. https://doi.org/10.1016/j.jallcom.2016.12.312.
[27] Egami T. Understanding the properties and structure of metallic glasses at the atomic level. JOM 2010;62:70–5. https://doi.org/10.1007/s11837-010-0036-4.